ACS APPLIED MATERIALS & INTERFACES

Research Article

www.acsami.org

Interference-free Micro/nanoparticle Cell Engineering by Use of High-Throughput Microfluidic Separation

David C. Yeo,[†] Christian Wiraja,[†] Yingying Zhou,[†] Hui Min Tay,[‡] Chenjie Xu,*[,†,§] and Han Wei Hou*[,‡]

[†]School of Chemical & Biomedical Engineering, Nanyang Technological University, 62 Nanyang Drive, Singapore 637459

[‡]Lee Kong Chian School of Medicine, Nanyang Technological University, 50 Nanyang Drive, Singapore 637553

[§]NTU-Northwestern Institute of Nanomedicine, Nanyang Technological University, 50 Nanyang Avenue, Singapore 639798

Supporting Information

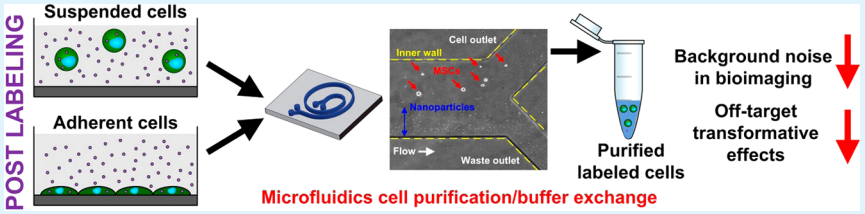

ABSTRACT: Engineering cells with active-ingredient-loaded micro/nanoparticles is becoming increasingly popular for imaging and therapeutic applications. A critical yet inadequately addressed issue during its implementation concerns the significant number of particles that remain unbound following the engineering process, which inadvertently generate signals and impart transformative effects onto neighboring nontarget cells. Here we demonstrate that those unbound micro/nanoparticles remaining in solution can be efficiently separated from the particle-labeled cells by implementing a fast, continuous, and high-throughput Dean flow fractionation (DFF) microfluidic device. As proof-of-concept, we applied the DFF microfluidic device for buffer exchange to sort labeled suspension cells (THP-1) from unbound fluorescent dye and dye-loaded micro/nanoparticles. Compared to conventional centrifugation, the depletion efficiency of free dyes or particles was improved 20-fold and the mislabeling of nontarget bystander cells by free particles was minimized. The microfluidic device was adapted to further accommodate heterogeneous-sized mesenchymal stem cells (MSCs). Complete removal of unbound nanoparticles using DFF led to the usage of engineered MSCs without exerting off-target transformative effects on the functional properties of neighboring endothelial cells. Apart from its effectiveness in removing free particles, this strategy is also efficient and scalable. It could continuously process cell solutions with concentrations up to 10^7 cells·mL^{-1} (cell densities commonly encountered during cell therapy) without observable loss of performance. Successful implementation of this technology is expected to pave the way for interference-free clinical application of micro/nanoparticle engineered cells.

KEYWORDS: *cell engineering, cell separation, nanoparticle, Dean flow fractionation, microfluidics*

INTRODUCTION

Engineering cells by agent-loaded micro/nanoparticles is a simple, genomic integration-free, and versatile method to imbue bioimaging capability and/or to augment/supplement its native therapeutic properties. Labeling cells with particle-based contrast agents enables the optimization of cell administration by monitoring cell biodistribution, status/function, and other activities post-transplantation.[1−3] For example, magnetic resonance imaging (MRI) successfully ascertains the accurate injection delivery of superparamagnetic iron oxide (SPIO) labeled dendritic cells as well as its migration behavior within cancer patient's lymph nodes.[4] Furthermore, engineering cells with microparticles containing transformative agents such as doxorubicin and antibodies can improve anti-cancer efficacy through targeted drug delivery and the manipulation of intracellular kinase activity.[5,6] Such means of cellular modification typically utilize either physical or chemical means to decorate various cell locations such as the plasma membrane or the cytoplasm.[7] Excess concentration levels of particles are usually supplied to saturate binding site(s), leaving significant quantities of unbound particles remaining in solution post-labeling. Remaining free particles confound precise identification of particle-engineered cells or potentially complicate therapeutic outcomes.[8,9] Free particles may cause cytotoxicity and interfere with other cells. Even bioimaging agents that are FDA-approved (e.g., indocyanine green) for various applications can be cytotoxic to certain cell types like retinal pigment epithelium.[10] Exposure to either transformative agents (growth factors, corticosteroids, etc.) at excessively high concentration levels or misdirected exposure (acting on nontarget cells) may induce unintended consequences (as shown herein). Even particulate carriers comprising "biocompatible" materials [e.g., poly(lactic-*co*-glycolic acid), PLGA] can incite potent immune cell responses under certain conditions.[11] Size, morphology, surface character-

Received: July 9, 2015
Accepted: September 1, 2015
Published: September 1, 2015

DOI: 10.1021/acsami.5b06167
ACS Appl. Mater. Interfaces 2015, 7, 20855−20864

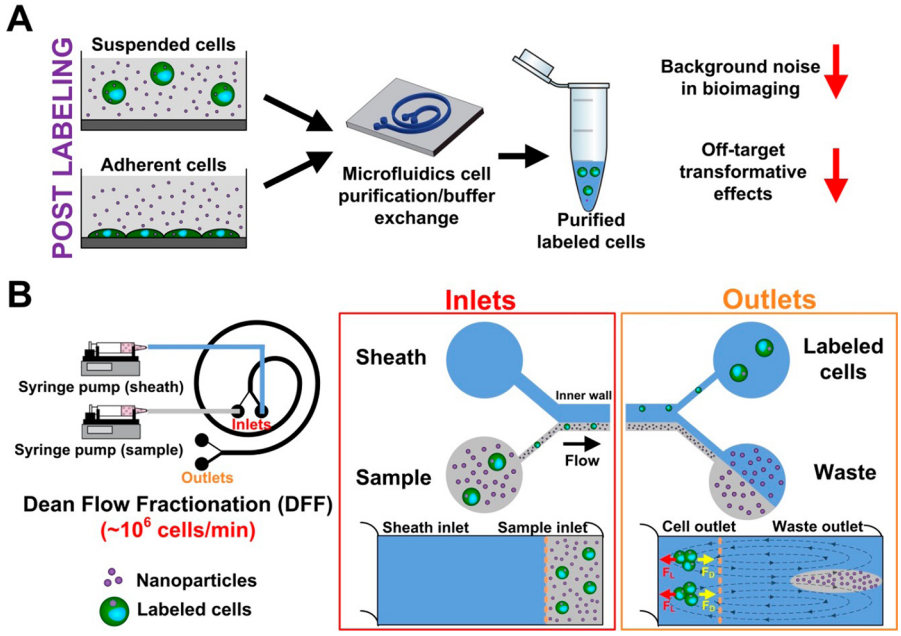

Figure 1. Application of Dean flow fractionation (DFF) for buffer exchange and nanoparticle removal in particle-based cell engineering. (A) Overall workflow for single-step nanoparticle (NP) removal from suspended and adherent cells postlabeling. Purified labeled cells have reduced bioimaging and off-target interference. (B) Schematic illustration of DFF in spiral device. The setup utilizes syringe pumps for continuous perfusion of labeled cells at high throughput ($\sim 10^{5-7}$·mL^{-1}). Under the influence of Dean drag forces (F_D, yellow arrows), labeled cells in NP-containing buffer solution migrate from the outer wall toward the inner wall. Larger cells experience additional strong inertial lift forces (F_L, red arrows) and focus near the microchannel inner wall while NPs and buffer solution recirculate to the outer wall. This facilitates the collection of labeled cells in buffer solution through the cell outlet, while NPs and other non-cell constituents are collected in the waste channel. Dotted lines (orange) indicate bifurcation positions between two inlets and outlets.

istics, and geometry are further particle design characteristics that determine the toxicity profile.[12] Furthermore, individuals suffering from autoimmune diseases (e.g., rheumatoid arthritis) have a greater proportion of T helper type I cells, which potentially delays nanoparticle systemic clearance.[13] Thus, removing free particles minimizes the toxicity profile and the risk of misdirected exposure to agent-loaded particles.

Conventional washing procedures do not always purify engineered cells completely. Conventional gradient centrifugation can separate engineered cells from free particles but is a laborious and fragmented process performed in batch. Moreover, shear stresses experienced by cells during high-speed centrifugation and the constituents of the density gradient medium may compromise cell integrity and/or influence cell behavior.[14] Microfluidic separation technologies are an attractive alternative. In recent years, several microfluidic strategies for continuous flow solution exchange have been reported, such as deterministic lateral displacement (DLD),[15] dielectrophoresis,[16,17] acoustophoresis,[18] and inertial microfluidics.[19−21] DLD microdevices have good separation resolution but suffer from low throughput (<1 μL·min^{-1}) and are prone to clogging issues within the micropillar array. Similarly, dielectrophoresis-based methods are low-throughput (~1−3 μL·min^{-1}) and require differences in intrinsic dielectrophoretic cell phenotypes or additional cell labeling steps to achieve separation.[16] Acoustophoretic particle washing achieves high buffer exchange efficiency (~99.98%) but is limited by low particle recovery (~75%).[18] A more promising approach involves inertial microfluidics—the lateral migration of particles or cells across streamlines to focus at distinct positions due to dominant lift forces (F_L) at high Reynolds number (Re)[22−24]—and have been employed for buffer exchange applications by switching particle focusing position in microchannels of different aspect ratios[19] or inducing inertial flow deformation by use of micropillars.[20,21] However, these techniques have poor solution exchange performance (~10−30% contaminant solution remains), as the separated cells usually remain close to the boundary between original and new buffer solutions.[19−21] More importantly, size distribution of target cells has to be similar to achieve precise inertial focusing and separation from original buffer solution and would be an issue, especially in processing of heterogeneous-sized cell types such as mesenchymal stem cells.[25]

Herein, we introduce a novel approach to efficiently remove unbound particles (<2 μm) from particle-engineered cells with high heterogeneity in cell size (10−30 μm) in a continuous and high-throughput manner (Figure 1). This is based on an inertial microfluidics technique termed Dean flow fractionation (DFF), previously developed for isolating circulating tumor cells (CTCs) in spiral microchannels.[26] Specifically, the mixture of engineered cells and free particles post labeling is injected into the outer wall inlet of a spiral microfluidic device at high throughput ($\sim 10^{6-7}$·mL^{-1}) while the inner wall inlet runs fresh buffer solution. Under the influence of Dean drag forces in spiral channels, cells in the mixture migrate laterally from the outer wall toward the inner wall. The larger-sized cells experience stronger inertial lift forces and focus near the microchannel inner wall, while the (smaller) free particles recirculate to the outer wall following the completion of a full "Dean cycle". This facilitates the collection of a pure population of particle-engineered cells into the cell outlet suspended in buffer solution, while unbound free particles are retrieved from the waste channel.

DFF buffer exchange microfluidic technology was first applied to sort labeled suspension cells (THP-1) from unbound fluorescent dye and/or micro/nanoparticles. Superior separation

DOI: 10.1021/acsami.5b06167
ACS Appl. Mater. Interfaces 2015, 7, 20855−20864

performance compared to conventional centrifugation was observed, and the mislabeling of nontarget bystander cells by the free particles was observed to be minimal. The microfluidic device was then adapted to further accommodate heterogeneous-sized mesenchymal stem cells (MSCs). By completely removing free particles, engineered MSCs did not exert off-target transformative effects on neighboring endothelial cells. This new cell purification strategy facilitates large-volume cell sorting and can process up to 10 million cells·mL^{-1}, a cell density amenable for regenerative medicine applications.

RESULTS AND DISCUSSION

Design Principles of Dean Flow Fractionation Microfluidic Purification. Fluid flow through a spiral channel generates centrifugal acceleration radiating outward, leading to two counter rotating Dean vortices forming in the top and bottom halves of the channel.[27] These transverse Dean flow patterns impose additional lateral drag forces (F_D) that provide superior separation resolution,[28−30] since both inertial lift and drag forces (F_L and F_D) scale nonlinearly with particle size. Their superposition (F_L/F_D) determines the particle's equilibrium axial position along the microchannel cross-section.

Based on this theory, a spiral DFF device was fabricated from polydimethylsiloxane (PDMS) consisting of a two-inlet, two-outlet spiral microchannel [500 μm (w) × 115 μm (h)] with a total length of ∼10 cm (Figure 1A). This length was used to ensure sufficient time for complete Dean migration and recirculation of nanoparticles toward the outer wall as discussed previously.[26] Because the equilibrium position of particles depends on the shortest channel dimension (microchannel height h) due to varying shear rates across the channel cross section ($a_p/h > 0.07$, where a_p is particle size), the channel height was fixed at 115 μm so that cells (typical size ∼15 μm) can experience inertial focusing ($a_p/h \sim 0.1$) and equilibrate at a position of <20% width (<100 μm) from the inner wall.[29,31] At these flow conditions, particles were similarly focused within 20% (<100 μm) of the opposite channel, adjacent to the outer wall. During operation, a mixture of cells and particles was perfused into the outer wall inlet (75 μm width) at 120 μL·min^{-1} while sheath fluid was perfused through the inner wall inlet (425 μm width) at a higher flow rate (10×, ∼1200 μL·min^{-1}) to confine the sample stream near the outer wall (Figure 1B). As the sample traverses the spiral channel, cells from the original sample solution experience F_D and migrate toward the inner wall. Larger cells equilibrate near the inner wall, while the sample solution continues flowing along the Dean vortices and recirculates toward the outer wall.[26] This allows the inertially-focused cells to be replaced with buffer (sheath fluid) and the sample solution (containing unbound particles) to be removed as waste. To achieve complete buffer exchange, the smaller cell outlet (150 μm) proximal to the inner wall is designed to recover the cell suspension, whereas the larger waste outlet (350 μm) ensures the removal of the non-cell fraction.

To determine the optimal flow conditions for complete recirculation of particles and original sample buffer to the channel outer wall, 2 μm beads were used to model Dean migration of the sample solution, as the beads are much smaller ($a_p/h \sim 0.017$) and would only be subjected to lateral Dean drag forces in our device. The Stokes number (Stk) for 2 μm particles in our system is ∼10^{-5} ($Stk = \tau/t_{rest}$, where $\tau = \rho_p d_p^2/18\mu_f$ and $t_{rest} \sim 2h^2/\nu$; μ_f is fluid viscosity; ρ_p and d_p are particle density and diameter, respectively; h is half channel height; and ν is kinematic viscosity).[32] Since $Stk \ll 1$, it is expected that the particles follow fluid streamlines closely. Bead solution and sheath fluid were pumped into the DFF device at a flow ratio of 1:10, and fluorescence imaging was used to capture their equilibrium position.

As shown in Figure 2A, the 2 μm beads migrated as a tight band under the influence of Dean vortices from the inner wall toward the outer wall as the perfusion speed increased. At a flow rate of 1000 μL·min^{-1} and above, all the 2 μm beads were collected in the large waste outlet. We then characterized the focusing and equilibrium positions of bead at other sizes (2, 5, 10, and 15 μm) under various flow rate conditions (Figure S1). To ensure efficient removal of free particles while minimizing any shear stress on processed cells, the flow rate was fixed at 1200 μL·min^{-1} for subsequent experiments. In addition to the flow rate, the specific properties of device design (encompassing channel

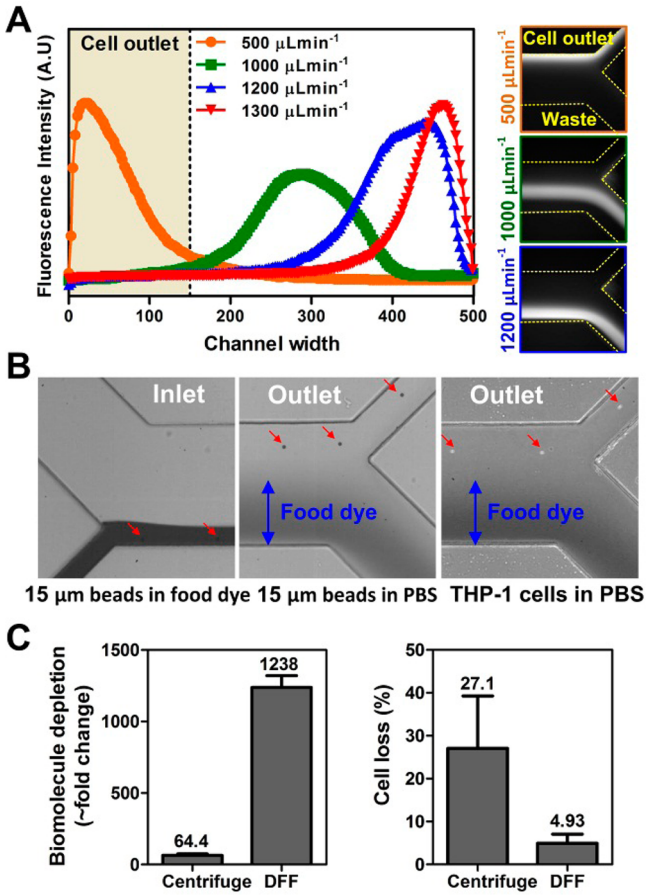

Figure 2. Buffer exchange via Dean flow fractionation (DFF). (A) Average fluorescence intensity line scans, showing the distribution of 2 μm beads across the channel width at increasing flow rates. Approximate position of the cell outlet (150 μm wide) at inner wall (origin) is indicated. Corresponding fluorescence images illustrating flow positions of 2 μm beads at different flow rates are also shown (yellow dashed lines indicate the approximate position of microchannel walls). (B) High-speed images at the inlet and outlet show efficient buffer exchange of representative biomolecule (food dye) solution with 15 μm beads and THP-1 cells. Food dye (dark colored, blue arrows) are recirculated to the outer wall and removed as waste, while inertially-focused beads and cells (red arrows) are replaced with sheath buffer and focused into the cell outlet. (C) Superior buffer exchange performance of DFF technology based on ∼20-fold increase in biomolecule depletion with lower cell loss (∼4.93%) compared to centrifugation. Values are $N = 3$, mean ± SD.

DOI: 10.1021/acsami.5b06167
ACS Appl. Mater. Interfaces 2015, 7, 20855−20864

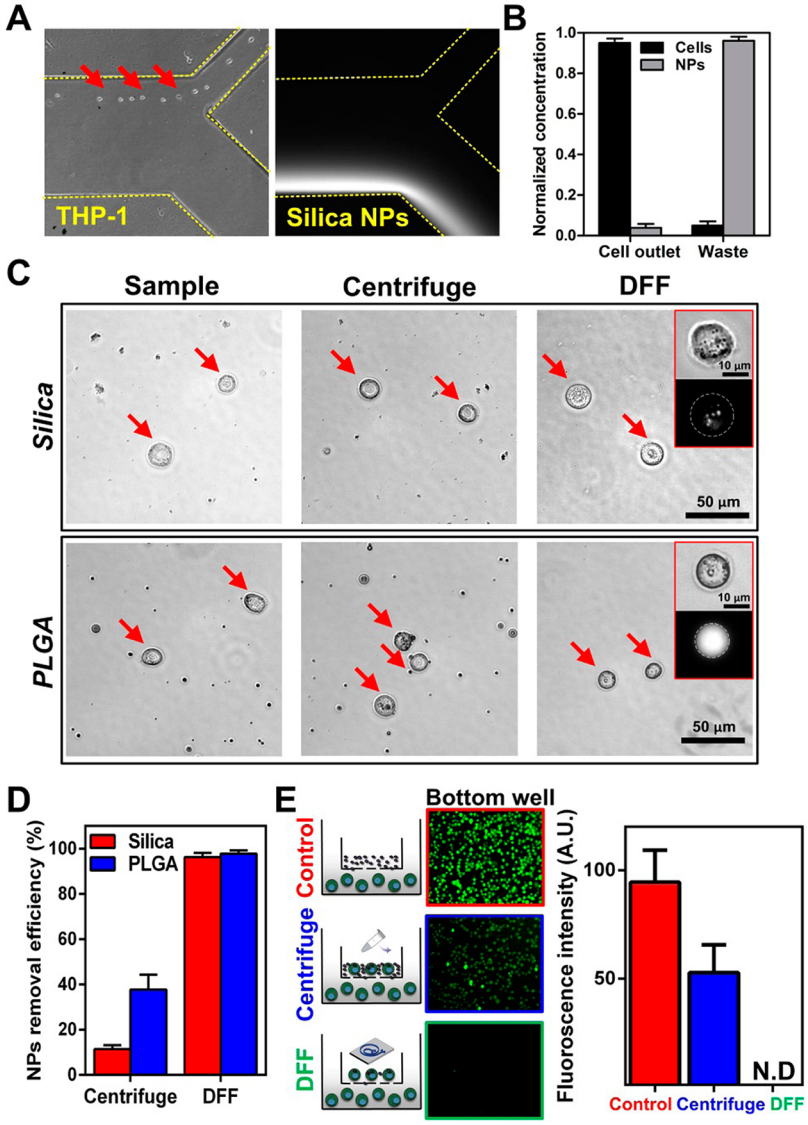

Figure 3. Nanoparticle removal from THP-1 cells via DFF. (A) High-speed and fluorescence images indicating distinct equilibrium positions of THP-1 cells (red arrows) and silica NPs loaded with calcein dye. Yellow dashed lines indicate the approximate position of the microchannel walls. (B) Separation performance of cells and silica NPs based on flow cytometry analysis. (C) Representative bright field images of purified labeled THP-1 cells (red arrows) and (D) NPs removal efficiency using centrifuge and DFF. (E) Non detectable fluorescence signal in unlabeled THP-1 cells at bottom well after 24 h coculture with DFF-purified labeled THP-1 (upper chamber) using Transwell assay (8.0 μm pores). In contrast, high fluorescence signals were detected in control (NPs only) and centrifuge-purified THP-1 cells. Values are $N = 3$, mean ± SD.

loops/cycles) are also crucial to maintain maximal separation between 2 and 10 μm beads. Changes to these parameters will compromise this separation distance and reduce efficiency in sorting free nano/microparticles from labeled cells.

Quantifying Dean Flow Fractionation Microfluidics Separation Efficacy. Next, suspension monocyte cells (THP-1) and 15 μm beads were mixed in a solution containing model biomolecules [food dye, ~800 Da, or fluorescein isothiocyanate (FITC)−dextran, 40 kDa] for buffer exchange experiments. These molecules are suitable for demonstrating solution exchange applications, as their high Peclet numbers (~1000−5000) indicate negligible diffusive effects[19] (Peclet equation[19]). Their molecular size range also encompasses a broad range of bioimaging and transformative agent payloads, from steroids (~500 Da) to proteins (~50−70 kDa), typically loaded into particles.[5,6] High-speed imaging clearly showed that both THP-1 cells and model 15 μm beads were focused and sorted into the cell outlet, while the food dye was directed to the outer region (Figure 2B). To quantify biomolecule depletion, food dye was substituted with FITC−dextran and nearly all the biomolecules were observed to have been removed, resulting in superior biomolecule depletion efficiency (20-fold) compared to the supernatant obtained from conventional centrifugation (Figure 2C). Moreover, DFF microfluidics exhibited more efficient purification performance with significantly lower cell loss (4.93%) compared to centrifugation (27.1%). This suggests that DFF purification efficiently removes larger nanoparticles (NPs) and microparticles used for cell labeling.

Efficient Purification of Labeled Suspension Cells. THP-1 cells were labeled with either silica (~500 nm) or poly(lactic-*co*-glycolic acid) (PLGA, ~ 1 μm) NPs through culture medium incubation. The efficacy of DFF purification of engineered suspension cells from free particles (silica and PLGA NPs) was next evaluated. Both particles were fluorescent due to

DOI: 10.1021/acsami.5b06167
ACS Appl. Mater. Interfaces 2015, 7, 20855−20864

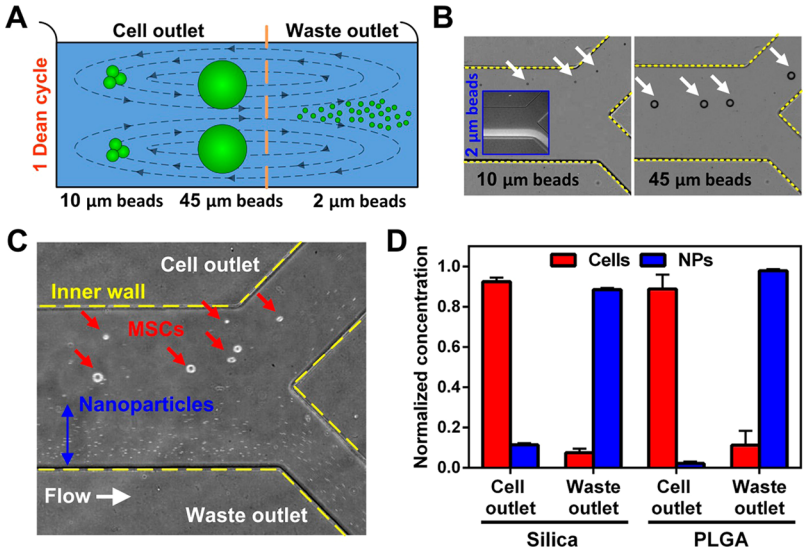

Figure 4. Unbound nanoparticle removal from mesenchymal stem cells (MSCs) via DFF. (A) Schematic of channel cross section indicating the approximate equilibrium position of different-sized beads. At optimized flow conditions, 10 μm beads are inertial-focused at the inner wall, while the 45 μm beads remain closer to the channel center as they experience significant Stokes drag, which impairs their migration to the inner wall. Beads of 2 μm (and consequently NPs) complete a recirculation back to the outer wall. (B) High-speed images confirm flow positions of 10 and 45 μm beads (white arrows). Inset fluorescence image (blue box) indicates the flow position of 2 μm beads at the same flow rate. (C) Representative high-speed image illustrating efficient separation of MSCs (red arrows) and PLGA NPs (blue arrows) into different outlets. Yellow dashed lines indicate the approximate position of the microchannel walls. (D) Separation performance of MSCs from silica and PLGA NPs. Values are $N = 3$, mean ± SD.

the encapsulation of organic dyes (calcein and calcein AM, respectively). The mixture of labeled cells and free particles (silica or PLGA NPs) was subsequently introduced into the spiral DFF separation device. Via high-speed imaging, efficient purification of THP-1 cells was observed, whereas fluorescence imaging showed that most of the unbound free silica NPs (containing calcein) were channeled into the waste outlet (Figure 3A). To quantify separation efficiency, flow cytometry was employed to analyze samples from both cell and waste outlets on the basis of their distinct forward and side scatter characteristics (Figure S2A). Compared with the unpurified samples, the cell outlet recovered the majority of THP-1 cells (95.1% ± 2.1%) with minimal silica NPs presence, whereas the waste outlet contained most of the NPs (95.2% ± 1.9%) (Figure 3B). Similarly efficient separation was also observed for THP-1 cells labeled with PLGA NPs (Figure S2B). Furthermore, cell recovery performance remained high (>90%) for both labeling methods when sample concentration was increased by 100-fold to 10^7 cells·mL^{-1} (Figure S3). This is a key improvement over existing inertial microfluidic cell separation methods, which are generally limited to 10^5 cells·mL^{-1} capacity due to cell−cell interaction and cell overcrowding at equilibrium positions[29]

Removal of unbound particles from labeled cells is not trivial, since common laboratory separation techniques cannot easily discriminate the constituents of a suspension solution containing different-sized particles (i.e., unbound particles and labeled cells). The separation efficiency between DFF and conventional centrifugation separation was then compared (Figure 3C). Before purification, representative images showed that inlet samples consisted of labeled cells suspended in a mixture of free NPs (silica or PLGA). Following centrifugation, the cell fraction still contained significant quantities of free particles, whereas free particles were barely seen following DFF purification. Fluorescence imaging showed that internalized NPs in the engineered THP-1 cells were well retained during DFF purification (insets). Flow cytometric analysis also revealed that centrifugation could remove only 11.4% ± 1.72% of free silica NPs and 37.7% ± 6.63% of free PLGA NPs (Figure 3D). In contrast, DFF was much more efficient, removing 96.2% ± 1.94% of free silica NPs and 97.8% ± 1.47% of free PLGA NPs. This clearly demonstrates DFF superior performance over conventional centrifugation in unbound NP removal, a byproduct from cell labeling.

A benefit of removing unbound particles from labeled cells is to minimize the mislabeling of nontarget bystander cells. This was assessed by a coculture assay with Transwell membranes, whose pores (8 μm) selectively allow unbound NPs to pass through, whereas cell−cell NP transfer is prevented. Unlabeled THP-1 cells were seeded in 24 wells before insertion of Transwell membranes to create a double-chambered well with an upper and lower deck. PLGA NP-labeled THP-1 cells were then seeded in the upper chamber (Figure 3E). After 6 h of incubation, free PLGA NPs from unpurified samples diffused through the inset membrane and labeled THP-1 cells seeded in the lower chamber. In the group where conventional centrifugation was used to purify particle-engineered THP-1 cells, significant fluorescence signal was observed in the lower chamber cell population that was unlabeled during experiment commencement. Fluorescence signal from these cells was expressed at ~50% that of control free NP cultures. Excitingly, no detectable fluorescent signal was emitted from these cells if the labeled cells from the upper chamber were purified by DFF, which demonstrated efficient removal of NPs loaded with fluorescence contrast agent.

Efficient Purification of Mesenchymal Stem Cells. We next adapted the microfluidic DFF technology to purify cells with greater therapeutic relevance. Unlike THP-1 cells, which are ~15 μm and relatively homogeneous in size, MSCs have a highly heterogeneous distribution, ranging between 16 and 28 μm in diameter.[25,33] In preclinical studies, they are also a popular candidate to engineer with micro/nanoparticles to track their biodistribution following implantation[34−36] or to endow augmented therapeutic properties.[37−40] To accommodate high

DOI: 10.1021/acsami.5b06167
ACS Appl. Mater. Interfaces 2015, 7, 20855−20864

cell recovery of the heterogeneous-sized MSCs, minor modifications were made to the spiral device dimensions and its operating characteristics. Specifically, the channel height was increased from 115 to 130 μm to enable inertial focusing of larger MSCs. The ratio between cell and waste outlet channels, key to the efficient collection of partitioned cells and unbound NPs, was determined by assessing particle focusing behavior between three different types of beads.

The adapted device was assessed with a mixture of 2, 10, and 45 μm beads: 10 and 45 μm beads represent the minimal and maximal MSC dimensions, while 2 μm beads represent unbound particles to be removed as waste. As discussed above (Figures 2 and 3), inertial focusing in the spiral channel tends to focus larger particles closer to the inner wall. However, 45 μm beads ($a_p/h \sim 0.35$) experienced significant Dean drag forces (Stokes drag; $F_D \sim a_p$) that slowed down their migration and prevented migration to the inner wall (Figure 4A). Thus, large beads (i.e., 10 and 45 μm beads) remained focused closer to the channel center while the smaller 2 μm beads completed a Dean cycle back to the outer wall and could be efficiently channeled into the waste outlet (Figure 4B). To facilitate efficient cell collection, the ratio between cell and waste outlet was modified to 3:2 (300 and 200 μm, respectively) as opposed to 3:7 (150 and 350 μm, respectively) during THP-1 cell purification.

The modified DFF microfluidic device was next used to purify MSCs. Similar to the above experiments with THP-1 cells, MSCs were labeled with silica or PLGA NPs. Following trypsin dissociation, the mixture was processed in the DFF spiral device. Figure 4C, a representative image during the purification of the MSC and PLGA NP mixture, distinctly showed that labeled MSCs were well separated from unbound particles. Efficient separation of MSCs from the particles can be better seen in the accompanying video (Supporting Information). High MSC recovery (~90%) was achieved at the cell outlet, and the removal of silica NPs and PLGA NPs into the smaller waste outlet was similarly efficient at 88.5% and 97.8%, respectively (Figure 4D).

Dean Flow Fractionation Microfluidic Purification Restores Endothelial Cell Migration. During THP-1 purification, we showed how the successful removal of free fluorescent particles from labeled cells minimized the mislabeling of nontarget bystander cells (Figure 3, above). In the case of MSCs, we shifted our focus to demonstrate that free particle removal from engineered cells could reduce undesirable interference with bystander cell function. Another significant difference between THP-1 and MSC purification is that the former are suspended whereas the latter are anchorage-dependent cells. Thus, the bulk of free particles from MSC labeling can be removed by washing/medium exchange. In this case, we evaluated whether DFF purification further reduced interference resulting from free particles that enter solution during processing (washing, dissociation, and collection) of adherent cells into a cell suspension.

Dexamethasone (DEX) is a widely used synthetic glucocorticoid compound. Although it has numerous benefits for MSC culture,[41−43] DEX can also interfere with endothelial cell migration, function, angiogenesis, and wound healing.[44,45] MSCs have been proposed as a cell-based carrier to achieve spatiotemporal controlled drug delivery by loading PLGA NPs with DEX (DEX-PLGA NPs).[37−39,45] Given its potent anti-inflammatory activity,[46,47] inadvertent introduction of free DEX-PLGA NPs alongside engineered MSCs may cause off-target effects, disrupting normal endothelial function.[48]

By use of the Transwell coculture system, human umbilical vein endothelial cells (HUVECs) were grown to confluence in the lower chamber before DEX-PLGA NP-labeled MSCs were seeded in the upper chamber. A scratch wound assay was performed on HUVECs just prior to seeding the labeled MSCs.[49] To visualize the migrating cells and DEX-PLGA NPs, HUVECs were labeled with the carbocyanine dye DiB (blue), whereas DEX-PLGA NPs were coloaded with red-shifted DiI dye (red). As shown in Figure 5, the extent of HUVEC migration after 24 h

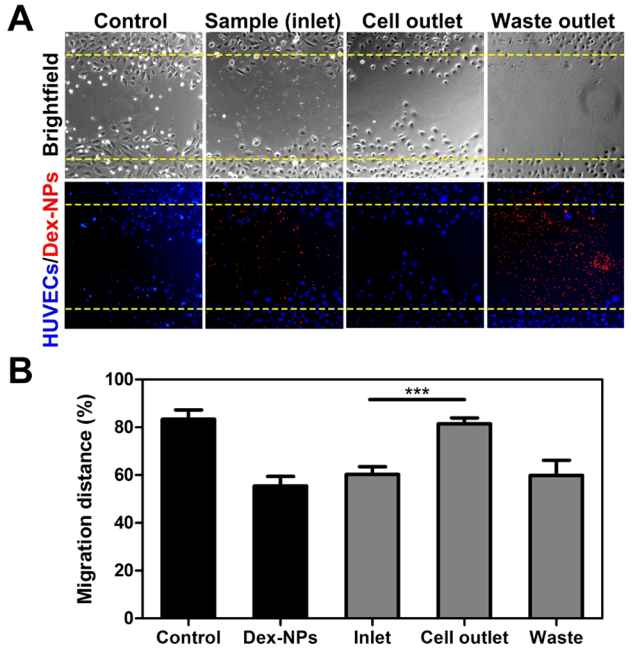

Figure 5. HUVEC migration assay after coculture with mesenchymal stem cells (MSCs) labeled with dexamethasone-loaded nanoparticles (DEX NPs). (A) Representative phase-contrast and fluorescence images of HUVEC migration after 24 h when cocultured with MSCs from control, inlet (before purification), and DFF-sorted (after purification) samples. Yellow dotted lines represent the original separation following the inflicted "wound" on the confluent cell monolayer at time = 0. Cells are stained blue with DiB, and DEX NPs are stained red with DiI. (B) Normalized migration distance under different conditions. A significant increase in migration distance was observed in HUVECs cocultured with DFF-purified MSCs from cell outlet as compared to inlet MSCs (containing free DEX NPs). Values are $N = 3$, mean ± SD. ***$P < 0.001$.

of coculture with unmodified MSCs was similar to those cocultured with DFF-purified DEX-PLGA NP-labeled MSCs. In both cases, HUVECs restored the separation distance by 80−85% within 24 h. Moreover, free DEX-PLGA NPs (red) were not visible when HUVECs were cocultured with DFF-purified labeled MSCs (Figure 5A). On the other hand, both DEX-PLGA NPs (waste) and unpurified DEX-PLGA NP-labeled MSCs (inlet) attenuated the migration distance of HUVECs to 55−60% (Figure 5B). Significant DEX-PLGA NPs (red signal) was also observed in the HUVEC samples cocultured with either the contents of the "waste" outlet (mainly DEX-PLGA NPs) or contents of the "inlet" (unpurified MSCs) (Figure 5A). This suggests that free particles were further released despite the washing/medium exchange when adherent MSCs were processed into a cell suspension. The presence of red particles in control and DFF-purified cells was not observed. Thus, DFF

DOI: 10.1021/acsami.5b06167
ACS Appl. Mater. Interfaces 2015, 7, 20855−20864

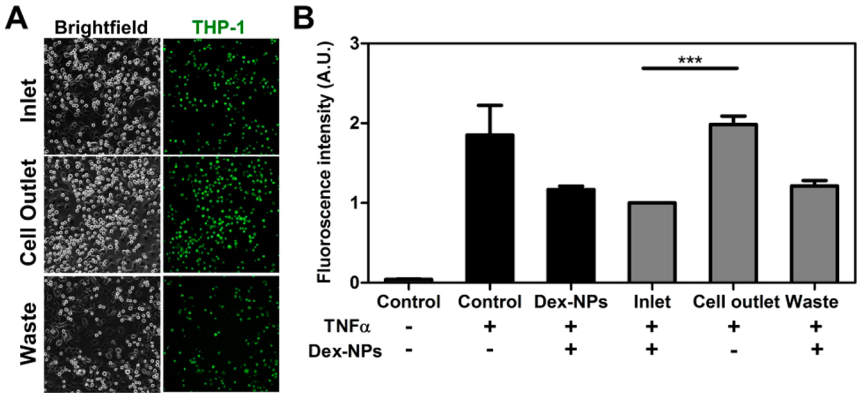

Figure 6. THP-1 adhesion assay after coculture with mesenchymal stem cells (MSCs) labeled with dexamethasone-loaded nanoparticles (DEX NPs). (A) Representative bright-field and fluorescence images of TNF-α-treated HUVEC monolayer, illustrating adhesion of THP-1 cells (stained with MitoGreen). (B) Normalized fluorescence signal indicating THP-1 cell adhesion to HUVEC monolayer when cocultured with MSCs from controls, inlet (before purification), and DFF-sorted (after purification) samples. A significant increase in THP-1 adhesion on HUVECs was observed when they were cocultured with DFF-purified MSCs from cell outlet as compared to inlet MSCs (containing free DEX NPs). Values are $N = 3$, mean ± SD. $^{***}P < 0.001$.

microfluidics efficiently purified labeled cells of free DEX-PLGA NPs to facilitate normal HUVEC migration.

Dean Flow Fractionation Microfluidic Purification Restores Endothelial–Leukocyte Cell Adhesion. We sought to investigate whether other endothelial cell functions apart from migration are impeded by exposure to the unbound DEX-PLGA NPs after MSC engineering. Leukocyte adhesion with endothelial cells is another critical function that facilitates immune cells' first response to bacterial infections and wound healing.[50] This physiological trait facilitates leukocyte adherence to mount an immune response. Endothelial–leukocyte cell adherence depends on the expression of adhesion molecules [endothelial leukocyte adhesion molecule 1 (ELAM-1), intercellular adhesion molecule 1 (ICAM-1), etc.[51]], which increase expression during exposure to inflammatory factors [e.g., tumor necrosis factor α (TNF-α)] for enhanced capture and binding between leukocytes and inflamed endothelial cells. However, misdirected anti-inflammatory DEX from free particles could inhibit endothelial–leukocyte cell adherence.

We next studied whether exposure to anti-inflammatory DEX from free NPs had any influence on leukocyte adhesion.[48,52,53] Moreover, we attempted to identify whether DFF purification would ameliorate this interference on bystander endothelial cells, if any. Transwell assays were used to coculture DEX-PLGA NP-engineered MSCs (upper chamber) with the HUVEC monolayer (lower chamber) for 24 h. Thereafter, HUVECs were treated with TNF-α for 4 h to stimulate inflammation, followed by the addition of MitoTracker Green-labeled THP-1 cells for adhesion. Unattached cells were stringently removed by thorough washing before imaging was performed immediately to determine the quantity of attached THP-1 cells. Acquired fluorescence signal was used to indirectly quantify attached monocytes.

As seen in Figure 6B, TNF-α treatment increased THP-1 adhesion on the HUVEC monolayer as judged by the ~45-fold increase in fluorescence emission, presumably through upregulated adhesion moieties.[54] However, when THP-1 cells were introduced after exposure to DEX-PLGA NPs ("waste" outlet), the fluorescence signal decreased by ~40%. Similar attenuation was observed when THP-1 cells were introduced to TNF-α-treated HUVECs together with unpurified MSCs. However, when DFF purification was performed to remove unbound DEX-PLGA NPs, the THP-1 cells retained adhesion with HUVECs. These results demonstrate how unbound anti-inflammatory DEX-PLGA NPs attenuate TNF-α stimulation of HUVECs and subsequently reduce THP-1 cell adhesion, which signifies interference with normal HUVEC behavior. On the other hand, efficient removal of unbound DEX-PLGA NPs by DFF purification removes interference and restores leukocyte–endothelial cell adhesion, a critical immune cell response.

CONCLUSIONS

Engineering cells with micro/nanoparticles is becoming a widely used, facile, and versatile method to enable cell tracking as well as augment native cell therapeutic properties. However, we reveal critical concerns regarding the unintentional transfer of imaging signal (PLGA-CAM) and transformative agents (DEX) onto bystander nontarget cells. Remnant NPs following cell labeling cannot be readily separated by conventional centrifugation. To address this issue, a novel cell purification strategy using inertial microfluidics in a spiral microchannel (DFF) was applied to efficiently remove unbound particles from labeled cells in a rapid, safe, and continuous manner. Unlike other inertial microfluidics-based buffer exchange strategies,[19−21] the developed DFF technique was able to exchange buffer solution from target cells with ultrahigh efficiency (>99.9%) due to the large channel width (500 μm) for buffer and small particles to migrate further away from the labeled cells prior separation.

The DFF microfluidic device operates at ultrahigh cell throughput ($\leq 10^6$ cells·min^{-1}) and has the requisite resolution and versatility to separate cells of differing dimensions merely through the minor adjustment of device geometry and operating conditions. This was evident during the transition from purifying homogeneous-sized monocytes to heterogeneous-sized MSCs. Furthermore, the process is scalable, since cell concentration can be increased 100-fold without compromising performance (Figure S3). We show that the inadvertent transfer of unbound particles to bystander nontarget cells is an undesirable trait that occurs as a result of cell labeling. Via DFF microfluidic purification, unbound fluorescent particles (silica and PLGA NPs) could be removed from monocytic suspension cells (THP-1), eliminating fluorescence signal transferred to unlabeled cells. Unbound particles loaded with transformative agents (e.g., DEX) also risk generating off-target effects. We showed that unpurified

DOI: 10.1021/acsami.5b06167
ACS Appl. Mater. Interfaces 2015, 7, 20855−20864

engineered MSCs containing unbound DEX-PLGA NPs attenuate physiological (migration assay) and pathological (leukocyte adhesion assay) responses in endothelial cells. Yet these properties were restored following DFF purification of DEX-PLGA NP-engineered MSCs.

Given that DFF microfluidics utilizes fluid mechanics (fluid flow and spiral design properties) as a basis for particle separation, it is unequipped to sort cells on the basis of expression of particular cellular properties. These could include cell surface markers, viability, or any other cell biomarkers. The inclusion of other sorting mechanisms that utilize "active" separation techniques such as magnetic, acoustic forces, and optical signals in combination with biomolecule recognition (e.g., antibodies, aptamers) can facilitate higher resolution separation of a given target cell population. While diminished cell viability due to shear stress from DFF is a possible source for concern, this is likely to be an unfounded concern due to the short residence time (<1 s) within the microfluidic channel. Previous studies using similar DFF separation devices also demonstrated no differences between cell viability for sorted and unsorted cells.[55]

In summary, conventional centrifugation has limited efficacy in removing unbound particles during cell engineering with micro/nanoparticles. Besides giving rise to false-positive imaging contrast, free drug-loaded particles also become inadvertently transferred to nontarget cells. DFF microfluidic technology offers an elegant and efficient solution to remove unbound micro/nanoparticles in a continuous manner. Its successful implementation allows the interference-free usage of particle-based cell engineering for therapy.

MATERIALS AND METHODS

Cell Culture. THP-1 cells (ATCC), a human monocytic cell line, were cultured in Roswell Park Memorial Institute (RPMI) 1640 medium (Lonza) supplemented with 10% fetal bovine serum (FBS; Gibco) and 0.05 mM 2-mercaptoethanol (Sigma). Human umbilical vein endothelial cells (HUVEC; Lonza) were cultured in endothelial cell growth medium (EGM) (Lonza) supplemented with 10% FBS. Meanwhile, mesenchymal stem cells (MSC; Lonza) were cultured in Dulbecco's modified Eagle's medium (DMEM; Lonza) supplemented with 10% FBS. They were all maintained at 37 °C in a humidified 5% CO_2 atmosphere and were fed thrice weekly.

Nanoparticle Fabrication. Silica NPs (~500 μm) were purchased from Sigma and loaded with calcein dye through overnight stirring (500 rpm) in concentrated calcein solution (200 μM). PLGA particles (i.e., CAM-PLGA, DEX-PLGA, and DEX/DiI-PLGA) were synthesized by a single emulsion procedure.[35] Initially, solutions containing either 250 μg of CAM, 10 mg of DEX, or 10 mg DEX with 20 μL of DiI (100 μM) in 2 mL of chloroform was mixed with 100 mg of PLGA (50:50) at 4 °C. Each mixture was then added dropwise to 3% (w/v) poly(vinyl alcohol) (PVA) aqueous solution before homogenization (Tissue Master 125, Omni International) at 24 000 rpm for 60 s. The emulsion was placed in the chemical hood for at least 3 h to allow chloroform evaporation. Finally, NPs were collected through centrifugation at 6000 rpm for 5 min and washed three times with double-distilled water before freeze-drying (−80 °C). Lyophilization was performed to prolong NP storage and samples were stored in −20 °C until just prior to usage.

Cell Labeling with Particles. Cells were seeded 24 h in advance at ≥80% confluency. Prior to cell labeling, CAM-PLGA NP (1 mg), silica NP (150 μg), DEX-PLGA (0.1 mg), or DEX/DiI-PLGA (0.1 mg) was incubated in 0.01% poly-L-lysine (PLL) solution (Sigma) at room temperature for 15−20 min. After centrifugation and removal of excess PLL supernatant, NPs were resuspended in 1 mL of culture medium and incubated together with cells for approximately 24 h (0.1 mg·mL^{-1} labeling concentration). Finally, the labeled cells were dissociated by use of trypsin (5 min, 37 °C) and collected for subsequent analysis.

Device Fabrication. The spiral microfluidic devices were fabricated by standard soft lithography methods with polydimethylsiloxane (PDMS).[26] Briefly, PDMS prepolymer was mixed with curing agent in a 10:1 ratio and silicon wafer patterned with channel design was used as template for replica molding. The PDMS mixture was cured after baking at 80 °C for 2 h and peeled from the master. Holes (1.5 mm) were punched for the inlets and outlets of the microchannels and the PDMS device was subsequently bonded to a 1-mm-thick glass slide by use of an air plasma machine (Harrick Plasma Cleaner).

Device Characterization. Fluorescent polystyrene beads (~10^{5-6}·mL^{-1}) of defined sizes (2, 5, 10, and 15 μm) were tested at different flow rates (1000, 1200, 1300, and 1400 μL·min^{-1}) and imaged by fluorescence microscopy. During operation, sample and sheath buffer, phosphate-buffered saline (PBS) containing 0.1% bovine serum albumin (BSA), were injected into the channel inlets at a flow ratio of 1:10 by separate syringe pumps (Chemyx Inc.). An inverted phase-contrast microscope (Nikon Eclipse Ti) with Metamorph software (Molecular Devices) was used to capture equilibrium positions of different bead sizes during flow. Once flow-rate conditions were optimized, mixtures of labeled cells with free particles were similarly injected into the device for separation, and phase-contrast bright-field videos were captured by use of a high-speed camera (Phantom V9.1).

Flow Cytometry. Eluents from both cell and waste outlets were collected and compared with inlet sample (~10^6 labeled cells·mL^{-1}) by use of flow cytometry ($N \geq 4$, with >10 000 events taken into account). For centrifuge comparison, the same cell samples were separately purified by conventional benchtop centrifugation (operated at 350*g*). A BD LSR Fortessa flow cytometer (BD Biosciences) was used to analyze the recovery of labeled cells and the removal efficiency of free particles.

Quantifying Biomolecule Depletion. To determine buffer exchange efficiency, FITC−dextran (40 kDa) solution (10 mg·mL^{-1}, Sigma−Aldrich) was processed by use of the spiral device. Eluents from the cell outlet and waste outlet were collected and analyzed on a microplate reader (BioTek). A standard fluorescence curve for predefined concentrations of FITC−dextran 40 was obtained, and biomolecule depletion factor was calculated on the basis of fluorescence signal of cell outlet/inlet sample ratio. For high-speed imaging, food dye (Apple green, molecular mass = 800 Da, 1:100) was used as a means to visualize lateral migration within the microchannel during DFF processing.

Transwell Assays. The experiments were typically performed by introducing a given condition of cells (e.g. unmodified sample, DFF-purified, centrifuge-purified, etc.) into the upper compartment to assess its effect on unlabeled cells (THP-1, HUVECs) in the lower compartment.

CAM-PLGA Nanoparticle Labeling Transwell Assay. To evaluate the usage of this device to prevent fluorescent particle transfer, THP-1 cells (~10^6 cells/mL) labeled with CAM-PLGA NP (1 mg·mL^{-1}) were seeded on 8 μm pore Transwells (Corning) that overlaid a layer of unlabeled THP-1 cells (~10^6 cells·mL^{-1}), prior to and after centrifugation as well as DFF free particle purification. Six hours postseeding, fluorescence images were obtained on a LX71 inverted fluorescent microscope (Olympus) and quantified for average cell fluorescent intensity by ImageJ software ($n \geq 200$ cells).

Migration Transwell Assay. DEX/DiI-PLGA NP (1 mg·mL^{-1}) labeled MSCs (~10^6 cells) were introduced to the Transwell assays with or without prior DFF purification. Prior to experimental commencement, a confluent layer of HUVECs below was scratched with 200 μL pipet tips along the entire length of a 24-well plate well to simulate a "wound" to facilitate HUVEC migration response.[49] The widths of the wounded area were measured after 12 and 24 h and normalized against the initial width to obtain the migration distances of the HUVECs (ImageJ). Additionally, the HUVECs on the bottom layer were stained with 4 μM DiB for 10−15 min to facilitate cellular boundary identification during fluorescent imaging.

Monocyte Adhesion Transwell Assay. Transwell inserts were placed on the top of a confluent layer of HUVECs. Each assay (24-well and insert) was seeded with dissociated DEX-PLGA NP-engineered MSCs (~10^6 cells) with and without DFF purification for 24 h. Transwell inserts were removed and HUVECs were treated with TNF-α (10 ng·

DOI: 10.1021/acsami.5b06167
ACS Appl. Mater. Interfaces 2015, 7, 20855−20864

mL^{-1} in EGM) for 4 h to induce inflammation. THP-1 monocytes were labeled with MitoTracker Green FM (100 nM, Invitrogen) at 37 °C for 30 min. Labeled THP-1 cells were then incubated at a density of 2×10^5 cells·$well^{-1}$ (500 μL of EGM) for an hour and imaged after thorough washing with PBS to remove any nonadherent cells. Fluorescence images were captured at 10× and 20× magnifications on a fluorescent microscope, and fluorescence signal intensity (indicative of THP-1 adherence) was quantified by use of ImageJ software.

■ ASSOCIATED CONTENT

Supporting Information

The Supporting Information is available free of charge on the ACS Publications website at DOI: 10.1021/acsami.5b06167.

Video showing efficient separation of MSCs from PLGA microparticles (AVI)

Optimization of microfluidic device flow rates, flow cytometric analysis, and effect of sample concentration on cell recovery (PDF)

■ AUTHOR INFORMATION

Corresponding Authors

*E-mail hwhou@ntu.edu.sg (H.W.H.).

*E-mail cjxu@ntu.edu.sg (C.J.).

Author Contributions

The manuscript was written through contributions of all authors. All authors have given approval to the final version of the manuscript. Specifically, D.C.Y., H.W.H., and C.X. conceived the project and wrote the manuscript. D.C.Y., C.W., Y.Z., H.M.T., and H.W.H. performed the experiments. H.W.H. prepared the figures.

Funding

This project was funded by NTU-Northwestern Institute of Nanomedicine (Nanyang Technological University). H.W.H. was supported by a Lee Kong Chian School of Medicine (LKC-Medicine, Singapore) postdoctoral fellowship.

Notes

The authors declare no competing financial interest.

■ ACKNOWLEDGMENTS

We acknowledge the kind gift of THP-1 cells and HUVECs from Dr. Mark Chong and assistance in microfabrication from Dr. Yuejun Kang and Nishanth V. Menon (School of Chemical and Biomedical Engineering, Nanyang Technological University).

■ REFERENCES

(1) Wiraja, C.; Yeo, D.; Lio, D.; Labanieh, L.; Lu, M.; Zhao, W.; Xu, C. Aptamer Technology for Tracking Cells' Status & Function. *Mol. Cell. Ther.* **2014**, *2*, 33.

(2) Yeo, D. C.; Wiraja, C.; Mantalaris, A.; Xu, C. Nanosensors for Regenerative Medicine. *J. Biomed. Nanotechnol.* **2014**, *10*, 2722−2746.

(3) Naumova, A. V.; Modo, M.; Moore, A.; Murry, C. E.; Frank, J. A. Clinical Imaging in Regenerative Medicine. *Nat. Biotechnol.* **2014**, *32*, 804−818.

(4) de Vries, I. J.; Lesterhuis, W. J.; Barentsz, J. O.; Verdijk, P.; van Krieken, J. H.; Boerman, O. C.; Oyen, W. J.; Bonenkamp, J. J.; Boezeman, J. B.; Adema, G. J.; Bulte, J. W.; Scheenen, T. W.; Punt, C. J.; Heerschap, A.; Figdor, C. G. Magnetic Resonance Tracking of Dendritic Cells in Melanoma Patients for Monitoring of Cellular Therapy. *Nat. Biotechnol.* **2005**, *23*, 1407−1413.

(5) Paulo, C. S. O.; Pires das Neves, R.; Ferriera, L. S. Nanoparticles for Intracellular-Targeted Drug Delivery. *Nanotechnology* **2011**, *22*, 494002.

(6) Stuckey, D. W.; Shah, K. Stem Cell-Based Therapies for Cancer Treatment: Separating Hope from Hype. *Nat. Rev. Cancer* **2014**, *14*, 683−691.

(7) Karp, J. M.; Zhao, W. *Micro- and Nanoengineering of the Cell Surface*, 1st ed.; William Andrew, an imprint of Elsevier: Oxford, U.K., San Diego, CA, and Waltham, MA, 2014.

(8) Soenen, S. J.; Rivera-Gil, P.; Montenegro, J.-M.; Parak, W. J.; De Smedt, S. C.; Braeckmans, K. Cellular Toxicity of Inorganic Nanoparticles: Common Aspects and Guidelines for Improved Nanotoxicity Evaluation. *Nano Today* **2011**, *6*, 446−465.

(9) Donaldson, K.; Poland, C. A. Nanotoxicity: Challenging the Myth of Nano-Specific Toxicity. *Curr. Opin. Biotechnol.* **2013**, *24*, 724−734.

(10) Gale, J. S.; Proulx, A. A.; Gonder, J. R.; Mao, A. J.; Hutnik, C. M. L. Comparison of the In Vitro Toxicity of Indocyanine Green to that of Trypan Blue in Human Retinal Pigment Epithelium Cell Cultures. *Am. J. Ophthalmol.* **2004**, *138*, 64−69.

(11) Veiseh, O.; Doloff, J. C.; Ma, M.; Vegas, A. J.; Tam, H. H.; Bader, A. R.; Li, J.; Langan, E.; Wyckoff, J.; Loo, W. S.; Jhunjhunwala, S.; Chiu, A.; Siebert, S.; Tang, K.; Hollister-Lock, J.; Aresta-Dasilva, S.; Bochenek, M.; Mendoza-Elias, J.; Wang, Y.; Qi, M.; Lavin, D. M.; Chen, M.; Dholakia, N.; Thakrar, R.; Lacik, I.; Weir, G. C.; Oberholzer, J.; Greiner, D. L.; Langer, R.; Anderson, D. G. Size- and Shape-Dependent Foreign Body Immune Response to Materials Implanted in Rodents and Non-Human Primates. *Nat. Mater.* **2015**, *14*, 643−651.

(12) Moghimi, S. M.; Hunter, A. C.; Andresen, T. L. Factors Controlling Nanoparticle Pharmacokinetics: An Integrated Analysis and Perspective. *Annu. Rev. Pharmacol. Toxicol.* **2012**, *52*, 481−503.

(13) Jones, S. W.; Roberts, R. A.; Robbins, G. R.; Perry, J. L.; Kai, M. P.; Chen, K.; Bo, T.; Napier, M. E.; Ting, J. P. Y.; DeSimone, J. M.; Bear, J. E. Nanoparticle Clearance is Governed by Th1/Th2 Immunity and Strain Background. *J. Clin. Invest.* **2013**, *123*, 3061−3073.

(14) Marchi, L.; Sesti-Costa, R.; Chedraoui-Silva, S.; Mantovani, B. Comparison of Four Methods for the Isolation of Murine Blood Neutrophils with Respect to the Release of Reactive Oxygen and Nitrogen Species and the Expression of Immunological Receptors. *Comp. Clin. Pathol.* **2014**, *23*, 1469−1476.

(15) Morton, K. J.; Loutherback, K.; Inglis, D. W.; Tsui, O. K.; Sturm, J. C.; Chou, S. Y.; Austin, R. H. Hydrodynamic Metamaterials: Microfabricated Arrays to Steer, Refract, and Focus Streams of Biomaterials. *Proc. Natl. Acad. Sci. U. S. A.* **2008**, *105*, 7434−7438.

(16) Hu, X.; Bessette, P. H.; Qian, J.; Meinhart, C. D.; Daugherty, P. S.; Soh, H. T. Marker-Specific Sorting of Rare Cells Using Dielectrophoresis. *Proc. Natl. Acad. Sci. U. S. A.* **2005**, *102*, 15757−15761.

(17) Cummings, E. B. Streaming Dielectrophoresis for Continuous-Flow Microfluidic Devices. *IEEE Eng. Med. Biol. Mag.* **2003**, *22*, 75−84.

(18) Augustsson, P.; Persson, J.; Ekstrom, S.; Ohlin, M.; Laurell, T. Decomplexing Biofluids Using Microchip Based Acoustophoresis. *Lab Chip* **2009**, *9*, 810−818.

(19) Gossett, D. R.; Tse, H. T. K.; Dudani, J. S.; Goda, K.; Woods, T. A.; Graves, S. W.; Di Carlo, D. Inertial Manipulation and Transfer of Microparticles Across Laminar Fluid Streams. *Small* **2012**, *8*, 2757−2764.

(20) Amini, H.; Sollier, E.; Masaeli, M.; Xie, Y.; Ganapathysubramanian, B.; Stone, H. A.; Di Carlo, D. Engineering Fluid Flow using Sequenced Microstructures. *Nat. Commun.* **2013**, *4*, 1826.

(21) Sollier, E.; Amini, H.; Go, D. E.; Sandoz, P. A.; Owsley, K.; Di Carlo, D. Inertial Microfluidic Programming of Microparticle-Laden Flows for Solution Transfer around Cells and Particles. *Microfluid. Nanofluid.* **2015**, *19*, 53−65.

(22) Hur, S. C.; Henderson-MacLennan, N. K.; McCabe, E. R. B.; Di Carlo, D. Deformability-based Cell Classification and Enrichment using Inertial Microfluidics. *Lab Chip* **2011**, *11*, 912−920.

(23) Mach, A. J.; Di Carlo, D. Continuous Scalable Blood Filtration Device Using Inertial Microfluidics. *Biotechnol. Bioeng.* **2010**, *107*, 302−311.

(24) Di Carlo, D.; Irimia, D.; Tompkins, R. G.; Toner, M. Continuous Inertial Focusing, Ordering, and Separation of Particles in Microchannels. *Proc. Natl. Acad. Sci. U. S. A.* **2007**, *104*, 18892−18897.

(25) Lee, W. C.; Shi, H.; Poon, Z.; Nyan, L. M.; Kaushik, T.; Shivashankar, G. V.; Chan, J. K. Y.; Lim, C. T.; Han, J.; Van Vliet, K. J. Multivariate Biophysical Markers Predictive of Mesenchymal Stromal

Cell Multipotency. *Proc. Natl. Acad. Sci. U. S. A.* **2014**, *111*, E4409−E4418.
(26) Hou, H. W.; Warkiani, M. E.; Khoo, B. L.; Li, Z. R.; Soo, R. A.; Tan, D. S.-W.; Lim, W.-T.; Han, J.; Bhagat, A. A. S.; Lim, C. T. Isolation and Retrieval of Circulating Tumor Cells using Centrifugal Forces. *Sci. Rep.* **2013**, *3*, 1259.
(27) Dean, W. The Stream-line Motion of Fluid in a Curved Pipe. *Philos. Mag. Series 7* **1928**, *5*, 673−695.
(28) Bhagat, A. A. S.; Kuntaegowdanahalli, S. S.; Papautsky, I. Continuous Particle Separation in Spiral Microchannels using Dean Flows and Differential Migration. *Lab Chip* **2008**, *8*, 1906−1914.
(29) Kuntaegowdanahalli, S. S.; Bhagat, A. A. S.; Kumar, G.; Papautsky, I. Inertial Microfluidics for Continuous Particle Separation in Spiral Microchannels. *Lab Chip* **2009**, *9*, 2973−2980.
(30) Wu, L.; Guan, G.; Hou, H. W.; Bhagat, A. A. S.; Han, J. Separation of Leukocytes from Blood Using Spiral Channel with Trapezoid Cross-Section. *Anal. Chem.* **2012**, *84*, 9324−9331.
(31) Martel, J. M.; Toner, M. Particle Focusing in Curved Microfluidic Channels. *Sci. Rep.* **2013**, *3*, 3340.
(32) Winer, M. H.; Ahmadi, A.; Cheung, K. C. In *Effects of Density Difference between Particles and Fluid on Inertial Focusing Positions in Transient Microflows*; 18th International Conference on Miniaturized Systems for Chemistry and Life Sciences, San Antonio, TX, 26−30 October 2014; 2462−2464.
(33) Caplan, A. I. Adult Mesenchymal Stem cells for Tissue Engineering Versus Regenerative Medicine. *J. Cell. Physiol.* **2007**, *213*, 341−347.
(34) Gao, Y.; Wang, Y.; Fu, A.; Shi, W.; Yeo, D.; Luo, K. Q.; Ow, H.; Xu, C. Tracking Mesenchymal Stem Cell Tumor-Homing using Fluorescent Silica Nanoparticles. *J. Mater. Chem. B* **2015**, *3*, 1245−1253.
(35) Xu, C.; Miranda-Nieves, D.; Ankrum, J. A.; Matthiesen, M. E.; Phillips, J. A.; Roes, I.; Wojtkiewicz, G. R.; Juneja, V.; Kultima, J. R.; Zhao, W.; Vemula, P. K.; Lin, C. P.; Nahrendorf, M.; Karp, J. M. Tracking Mesenchymal Stem Cells with Iron Oxide Nanoparticle Loaded Poly(lactide-co-glycolide) Microparticles. *Nano Lett.* **2012**, *12*, 4131−4139.
(36) Jokerst, J. V.; Khademi, C.; Gambhir, S. S. Intracellular Aggregation of Multimodal Silica Nanoparticles for Ultrasound-Guided Stem Cell Implantation. *Sci. Transl. Med.* **2013**, *5*, 177ra35.
(37) Ankrum, J. A.; Dastidar, R. G.; Ong, J. F.; Levy, O.; Karp, J. M. Performance-Enhanced Mesenchymal Stem Cells via Intracellular Delivery of Steroids. *Sci. Rep.* **2014**, *4*, 4645.
(38) Sarkar, D.; Ankrum, J. A.; Teo, G. S.; Carman, C. V.; Karp, J. M. Cellular and Extracellular Programming of Cell Fate Through Engineered Intracrine-, Paracrine-, and Endocrine-like Mechanisms. *Biomaterials* **2011**, *32*, 3053−3061.
(39) Bernardino, L.; Eiriz, M. F.; Santos, T.; Xapelli, S.; Grade, S.; Rosa, A. I.; Cortes, L.; Ferreira, R.; Bragança, J.; Agasse, F.; Ferreira, L.; Malva, J. O. Histamine Stimulates Neurogenesis in the Rodent Subventricular Zone. *Stem Cells* **2012**, *30*, 773−784.
(40) Li, L.; Tang, F.; Liu, H.; Liu, T.; Hao, N.; Chen, D.; Teng, X.; He, J. In Vivo Delivery of Silica Nanorattle Encapsulated Docetaxel for Liver Cancer Therapy with Low Toxicity and High Efficacy. *ACS Nano* **2010**, *4*, 6874−6882.
(41) Song, I.-H.; Caplan, A. I.; Dennis, J. E. Dexamethasone Inhibition of Confluence-Induced Apoptosis in Human Mesenchymal Stem Cells. *J. Orthop. Res.* **2009**, *27*, 216−221.
(42) Xiao, Y.; Peperzak, V.; van Rijn, L.; Borst, J.; de Bruijn, J. D. Dexamethasone Treatment during the Expansion Phase Maintains Stemness of Bone Marrow Mesenchymal Stem Cells. *J. Tissue Eng. Regener. Med.* **2010**, *4*, 374−386.
(43) Koehler, K. C.; Alge, D. L.; Anseth, K. S.; Bowman, C. N. A Diels−Alder Modulated Approach to Control and Sustain the Release of Dexamethasone and Induce Osteogenic Differentiation of Human Mesenchymal Stem Cells. *Biomaterials* **2013**, *34*, 4150−4158.
(44) Logie, J. J.; Ali, S.; Marshall, K. M.; Heck, M. M. S.; Walker, B. R.; Hadoke, P. W. F. Glucocorticoid-Mediated Inhibition of Angiogenic Changes in Human Endothelial Cells Is Not Caused by Reductions in Cell Proliferation or Migration. *PLoS One* **2010**, *5*, e14476.
(45) Shikatani, E. A.; Trifonova, A.; Mandel, E. R.; Liu, S. T.; Roudier, E.; Krylova, A.; Szigiato, A.; Beaudry, J.; Riddell, M. C.; Haas, T. L. Inhibition of Proliferation, Migration and Proteolysis Contribute to Corticosterone-Mediated Inhibition of Angiogenesis. *PLoS One* **2012**, *7*, e46625.
(46) Hickey, T.; Kreutzer, D.; Burgess, D. J.; Moussy, F. Dexamethasone/PLGA Microspheres for Continuous Delivery of an Anti-Inflammatory Drug for Implantable Medical Devices. *Biomaterials* **2002**, *23*, 1649−1656.
(47) Tsurufuji, S.; Sugio, K.; Takemasa, F. The Role of Glucocorticoid Receptor and Gene Expression in the Anti-Inflammatory Action of Dexamethasone. *Nature* **1979**, *280*, 408−410.
(48) Salvador, E.; Shityakov, S.; Förster, C. Glucocorticoids and Endothelial Cell Barrier Function. *Cell Tissue Res.* **2014**, *355*, 597−605.
(49) Liang, C. C.; Park, A. Y.; Guan, J. L. In Vitro Scratch Assay: a Convenient and Inexpensive Method for Analysis of Cell Migration In Vitro. *Nat. Protoc.* **2007**, *2*, 329−333.
(50) Roos, D.; Law, S. K. Hematologically Important Mutations: Leukocyte Adhesion Deficiency. *Blood Cells, Mol., Dis.* **2001**, *27*, 1000−1004.
(51) Ley, K.; Laudanna, C.; Cybulsky, M. I.; Nourshargh, S. Getting to the Site of Inflammation: the Leukocyte Adhesion Cascade Updated. *Nat. Rev. Immunol.* **2007**, *7*, 678−689.
(52) Cronstein, B. N.; Kimmel, S. C.; Levin, R. I.; Martiniuk, F.; Weissmann, G. A Mechanism for the Antiinflammatory Effects of Corticosteroids: the Glucocorticoid Receptor Regulates Leukocyte Adhesion to Endothelial Cells and Expression of Endothelial-Leukocyte Adhesion Molecule 1 and Intercellular Adhesion Molecule 1. *Proc. Natl. Acad. Sci. U. S. A.* **1992**, *89*, 9991−9995.
(53) Mulligan, M. S.; Varani, J.; Dame, M. K.; Lane, C. L.; Smith, C. W.; Anderson, D. C.; Ward, P. A. Role of Endothelial-Leukocyte Adhesion Molecule 1 (ELAM-1) in Neutrophil-Mediated Lung Injury in Rats. *J. Clin. Invest.* **1991**, *88*, 1396−1406.
(54) Iademarco, M. F.; Barks, J. L.; Dean, D. C. Regulation of Vascular Cell Adhesion Molecule-1 Expression by IL-4 and TNF-alpha in Cultured Endothelial Cells. *J. Clin. Invest.* **1995**, *95*, 264−271.
(55) Lee, W. C.; Bhagat, A. A. S.; Huang, S.; Van Vliet, K. J.; Han, J.; Lim, C. T. High-throughput Cell Cycle Synchronization Using Inertial Forces in Spiral Microchannels. *Lab Chip* **2011**, *11*, 1359−1367.

DOI: 10.1021/acsami.5b06167
ACS Appl. Mater. Interfaces 2015, 7, 20855−20864